CHEMISTRY OF MATERIALS
Article

Chem. Mater. **2010,** *22,* 869–875 869
DOI:10.1021/cm9016672

Microstructure and Thermoelectric Properties of Mechanically Robust PbTe-Si Eutectic Composites†

Joseph R. Sootsman,‡ Jiaqing He,§ Vinayak P. Dravid,§ Sedat Ballikaya,∥ Derek Vermeulen,∥ Ctirad Uher,∥ and Mercouri G. Kanatzidis*,‡,⊥

‡*Department of Chemistry and* §*Materials Science and Engineering, Northwestern University, Evanston, Illinois 60208,* ∥*Department of Physics, University of Michigan, Ann Arbor, Michigan 48109, and* ⊥*Materials Science Division, Argonne National Laboratory, Argonne, Illinois 60439*

Received June 16, 2009. Revised Manuscript Received August 22, 2009

The microstructure and thermoelectric properties of the PbTe-Si eutectic system are presented in detail. When rapidly quenched from the melt this system yields materials with thermoelectric properties similar to PbTe itself but with improved mechanical properties. Doping optimization was performed using PbI_2 as an n-type dopant giving precise control of the thermoelectric properties. Electron microscopy indicates that the PbTe-Si system is both a nanocomposite and microcomposite. Despite the added Si, the thermal conductivity of this composite follows closely that of PbTe. The temperature dependence of the Lorenz number was estimated, and it shows a significant departure from the value of metals (L_0) reaching only 45% of L_0 at 650 K. The optimized ZT for the PbTe-Si(8%) eutectic was 0.9 at 675 K. The improved mechanical robustness of these composites makes them attractive for use in large scale thermoelectric device fabrication.

Introduction

Thermoelectric (TE) power generation from vehicle waste heat is projected to improve gas mileage in internal combustion engines by as much as 10%.[1] To realize this goal, the efficiency of thermoelectric materials and systems must be improved. The efficiency of a thermoelectric device is determined by the temperature differential across the TE materials and the figure of merit of the TE materials themselves. The TE figure of merit is determined by the electrical and thermal transport behavior of the semiconductor and is defined as $ZT = S^2\sigma T/\kappa$ where S is the Seebeck coefficient, σ the electrical conductivity, κ the thermal conductivity, and T the temperature.[2,3] Recently, efforts to improve ZT have focused on preparing natural and artificial nanostructures to reduce the thermal conductivity by boundary scattering. For example, a number of bulk semiconductor nanocomposites prepared via spinodal decomposition,[4] matrix encapsulation,[5,6] and precipitation and growth[4,7−11] showing enhanced ZT have greatly increased interest in these mechanisms as methods to prepare thermoelectrics. An additional mechanism based on eutectic phase transformations is also of interest in preparing thermoelectric materials.

We suggest that eutectic mixtures are attractive as thermoelectrics (TE) because of their unique microstructure that allows for enhanced mechanical strength. This increase in mechanical strength is primarily due to their inhibition of crack propagation.[12] Additional benefits come from the ability to rapidly prepare materials and even the possibility to reduce thermal conductivity.[13] In fact, a number of eutectic materials based on III−V and IV−VI compound semiconductors have been studied previously as thermoelectrics.[14−22] Recently, we reported

† Accepted as part of the 2010 "Materials Chemistry of Energy Conversion Special Issue".

(1) Bell, L. E. *Science* **2008**, *321*(5895), 1457–1461.
(2) Rowe, D. M. *CRC Handbook of Thermoelectrics*; CRC Press: Boca Raton, FL, 1995; p 701.
(3) Rowe, D. M. *Thermoelectrics Handbook: Macro to Nano*; CRC/Taylor & Francis: Boca Raton, 2006.
(4) Androulakis, J.; Lin, C.-H.; Kong, H.-J.; Uher, C.; Wu, C.-I.; Hogan, T.; Cook, B. A.; Caillat, T.; Paraskevopoulos, K. M.; Kanatzidis, M. G. *J. Am. Chem. Soc.* **2007**, *129*(31), 9780–9788.
(5) Sootsman, J. R.; Pcionek, R. J.; Kong, H. J.; Uher, C.; Kanatzidis, M. G. *Chem. Mater.* **2006**, *18*(21), 4993–4995.
(6) Sootsman, J. R.; Kong, H.; Uher, C.; D'Angelo, J. J.; Wu, C.-I.; Hogan, T. P.; Caillat, T.; Kanatzidis, M. G. *Angew. Chem., Int. Ed. Engl.* **2008**, *47*, 1–6.
(7) Hsu, K. F.; Loo, S.; Guo, F.; Chen, W.; Dyck, J. S.; Uher, C.; Hogan, T.; Polychroniadis, E. K.; Kanatzidis, M. G. *Science* **2004**, *303*(5659), 818–821.
(8) Androulakis, J.; Hsu, K. F.; Pcionek, R.; Kong, H.; Uher, C.; D'Angelo, J. J.; Downey, A.; Hogan, T.; Kanatzidis, M. G. *Adv. Mater.* **2006**, *18*(9), 1170–1173.
(9) Poudeu, P. F. P.; D'Angelo, J.; Downey, A. D.; Short, J. L.; Hogan, T. P.; Kanatzidis, M. G. *Angew. Chem., Int. Ed. Engl.* **2006**, *45*(23), 3835–3839.
(10) Quarez, E.; Hsu, K. F.; Pcionek, R.; Frangis, N.; Polychroniadis, E. K.; Kanatzidis, M. G. *J. Am. Chem. Soc.* **2005**, *127*, 9177.
(11) Poudeu, P. F. P.; D'Angelo, J.; Kong, H.; Downey, A.; Short, J. L.; Pcionek, R.; Hogan, T. P.; Uher, C.; Kanatzidis, M. G. *J. Am. Chem. Soc.* **2006**, *128*(44), 14347–14355.
(12) Askeland, D. R.; Phule, P. P. *The Science and Engineering of Materials*, 4th ed.; Thomson: Pacific Grove, CA, 2003.
(13) Elliott, R. *Eutectic Solidification Processing Crystalline and Glassy Alloys*; Butterworths & Co: London, 1983.
(14) Isakov, G. I. *Semiconductors* **2005**, *39*(7), 738–741.
(15) Isakov, G. I. *J. Eng. Phys. Thermophys.* (*Translation of Inzhenerno-Fizicheskii Zhurnal*) **2004**, *77*(5), 1062–1068.
(16) Aliev, M. I.; Isakov, G. I.; Emin-Zade, A. T. *Neorg. Mater* **1985**, *21*(11), 1890–1893.
(17) Dement'ev, I. V.; Leonov, V. V. *Neorg. Mater* **1988**, *24*(1), 24–27.
(18) Leonov, V. V.; Gantimurova, Z. K. *Neorg. Mater* **1987**, *23*(11), 1915–1917.
(19) Leonov, V. V.; Chunarev, E. N. *Neorg. Mater* **1980**, *16*(10), 1753–1756.
(20) Leonov, V. V.; Spektor, Y. E. *Neorg. Mater* **1980**, *16*(8), 1358–1360.
(21) Ikeda, T.; Collins, L. A.; Ravi, V. A.; Gascoin, F. S.; Haile, S. M.; Snyder, G. J. *Chem. Mater.* **2007**, *19*(4), 763–767.
(22) Ikeda, T.; Azizgolshani, H.; Haile, S. M.; Snyder, G. J.; Ravi, V. A. *Int. Conf. Thermoelectr.* **2005**, *24*, 132–135.

Published on Web 09/11/2009

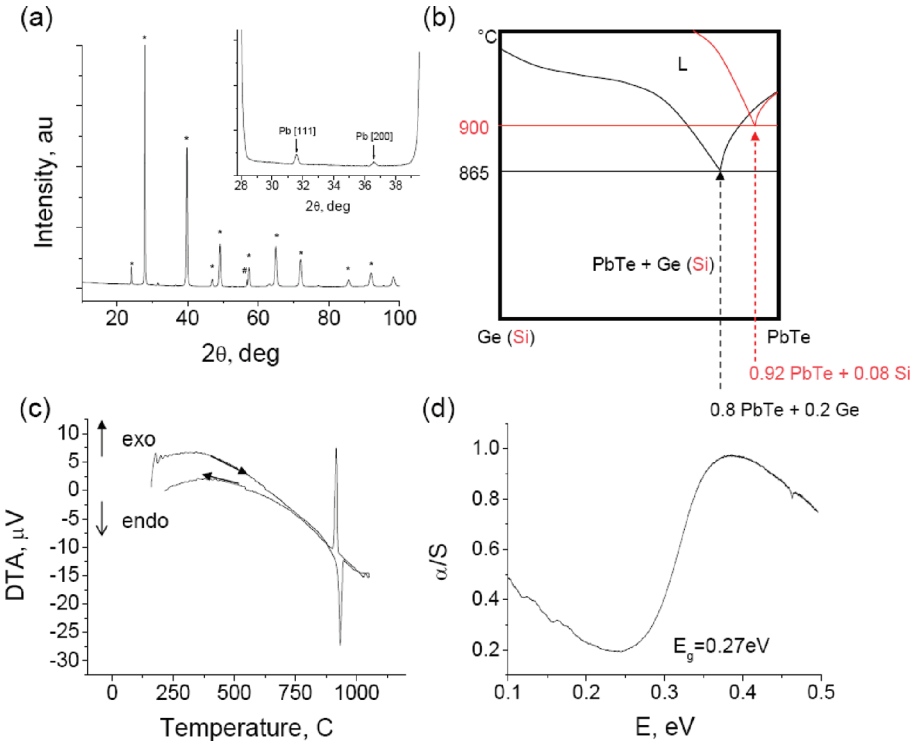

Figure 1. (a) Powder X-ray diffraction showing the major PbTe (* symbols) and Si reflection (# symbol) and the minor phase Pb precipitates (inset). (b) Phase diagram comparison for the PbTe-Ge system (black)[24] and the PbTe-Si system (red)[25] indicating the shift in eutectic composition and temperature at which the eutectic point occurs. (c) Heating and cooling differential thermal analysis curves indicating melting and recrystallization at ~927 °C. (d) Infrared absorption curve for PbTe-Si(8%) showing the E_g of 0.27 eV comparable to PbTe itself.

on the thermoelectric properties of the PbTe-Ge eutectic system and its analogue PbTe-$Ge_{1-x}Si_x$.[23] The eutectic point in this system occurs at the PbTe-Ge(20%) composition (Figure 1b).[24] Interestingly the large fraction of Ge did not increase the thermal conductivity as could be expected if the material followed a simple law of mixtures. In fact, when the second phase content was decreased and Ge was alloyed with Si, an improved ZT of 1.3 was obtained for the PbTe-$Ge_{0.8}Si_{0.2}$(5%) composite compared to ~0.8 for PbTe itself, primarily because of a reduced thermal conductivity.

The microstructure and thermoelectric properties of the germanium-free system PbTe-Si(8%) is reported in detail here. The eutectic point in this system occurs at a lower percentage of the minor phase (8% vs 20%) and occurs at a higher temperature than in the Ge system (900 °C vs 865 °C).[24,25] The low concentration of silicon as well as its lower cost compared to Ge make this eutectic system attractive for development as a thermoelectric. The carrier concentration and therefore the Seebeck coefficient and electrical conductivity could be precisely controlled by doping with PbI_2. The electron mobility of the PbTe-Si(8%) samples was high (~1000 $cm^2/(V\ s)$) and was not significantly reduced compared to that of pure PbTe by the Si precipitates. We show that a complex micro- and nanostructure contribute to reducing the well-known brittleness of PbTe without significantly increasing the lattice thermal conductivity. Rather, the latter follows closely with the expected value for PbTe, and we obtain ZT values comparable to PbTe with the benefit of having a rapidly prepared material and improved mechanical strength. The apparent mechanical robustness of the samples, the rapid synthesis, and the moderate ZT of these materials makes them attractive for module fabrication.

Experimental Section

Synthesis. Lead (Rotometals, 99.99%) and tellurium (Atlantic Metals, 99.999%) were combined in a 1:1 ratio in 25.4 mm diameter fused silica tube, sealed under vacuum, and heated to 1000 °C. For example, approximately 250 g of pure PbTe was prepared by quenching the resulting melt of Pb (149.4931 g, 0.7215 mol) and Te (92.0629 g, 0.7215 mol) in a room temperature water bath.

The resulting PbTe, Si (Cerac, 99.992%), and PbI_2 (Aldrich, 99.999%) were combined in the appropriate molar ratio in quartz tubes (8 mm ID) and sealed under vacuum. For example, 9.1623 g (0.0273 mol) of PbTe, 0.0672 g (0.0023 mol) of Si, and 0.0016 g (3.47×10^{-6} mol) of PbI_2 were used to prepare the PbTe-Si(8%) sample doped with 0.0127% PbI_2. The material was then heated to 1050 °C and allowed to homogenize in the melt for 12 h. The liquid was then rapidly cooled in a room temperature water bath.

The resulting ingots (8 mm diameter) were cut using a diamond blade saw into several pieces for electrical, thermal, and microstructural characterization. First a coin 8 mm in diameter and 2 mm thick was cut for thermal diffusivity measurements. The faces of the coin were polished to ensure

(23) Sootsman, J. R.; He, J.; Dravid, V. P.; Li, C.-P.; Uher, C.; Kanatzidis, M. G. *J. Appl. Phys.* **2009**, *105*(8), 083718/1–083718/8.
(24) Burmistrova, N. P.; Fitseva, R. G.; Faizullina, N. R.; Mullina, V. A. *Neorg. Mater* **1982**, *18*(5), 876–877.
(25) Odin, I. N. *Zh. Neorg. Khim.* **1994**, *39*(10), 1730–3.

they were parallel using 800 grit sandpaper. Adjacent to this coin a ~10 mm long cylinder was cut from which two samples were prepared. One ~3 × 3 × 10 mm and one 1 × 3 × 8 mm sample were prepared for electrical transport measurements and Hall effect measurement, respectively. These samples were cut using the diamond saw and polished using 800 grit sandpaper to provide the parallelepipeds necessary for measurements. All transport measurements were therefore conducted in the same direction along the length of the ingot.

Powder X-ray Diffraction. Powder X-ray diffraction experiments were performed on finely ground powders using an Inel diffractometer (Cu Kα radiation) operating at 40 kV/20 mA.

Electron Microscopy. Scanning electron microscopy was performed on highly polished samples using a Hitachi S3400 and S4800 with varying accelerating voltages for imaging and a 20 kV accelerating voltage for energy dispersive spectroscopy measurements.

Samples for transmission electron microscopy were prepared by conventional techniques of thinning, dimpling, and ion milling to obtain thin samples for analysis, as described previously in detail.[23] Microscopy was performed using a JEOL 2100F transmission electron microscope operating at a 200 keV accelerating voltage. Self-consistent ab initio multiple-scattering calculations for electron energy loss spectroscopy (EELS) were performed using the FEFF8.4 code to determine the energy loss spectrum of oxygen in SiO_2.[26]

Electrical Transport Characterization. Temperature dependent electrical conductivity and Seebeck effect measurements were performed using a ULVAC Technologies ZEM3. The electrical conductivity was determined using a four-probe method with spring loaded current contacts. Type R thermocouples double as both temperature sensors and voltage leads during measurements of the Seebeck coefficient. We used temperature gradients of 5, 10, and 15 °C and the corresponding voltage differences and temperature differences were then averaged. A temperature stability of 0.25° was maintained over the course of the measurement at each temperature step.

High temperature (300−750 K) Hall effect measurements were performed on samples ~1 × 3 × 8 mm in size with pressure contacts. The measurements were performed in a homemade apparatus under Ar atmosphere utilizing an Oxford Superconducting Magnet with constant magnetic field of ±1 T. The Hall resistance was monitored with Linear Research AC Resistance Bridge (LR-700).

Thermal Conductivity/Diffusivity Characterization. A Netzsch LFA-457 was used to measure temperature dependent thermal diffusivity and heat capacity in the range 300−700 K. Coins 8 mm in diameter and 2−2.5 mm thick were used in all measurements, and the thermal conductivity in these samples was determined using the laser flash diffusivity heat capacity method from 300 to 700 K. The diffusivity (D), density (ρ), and specific heat (C_p) were measured, and the total thermal conductivity was calculated using the formula $\kappa = D\rho C_p$.

Results and Discussion

Synthesis and Microstructural Characterization. The PbTe-Si eutectics can be rapidly prepared by comelting PbTe and Si in the appropriate ratios in fused silica ampules under vacuum to 1050 °C. The melts were then rapidly solidified by removing the ampules from the furnace and placing them inside a room temperature water bath. The resulting ingots are mechanically robust and were easily cut and polished for measurement.

Recently, the mechanical properties of PbTe have been studied in detail as these are important for reliable device fabrication.[27−29] Generally, PbTe is a brittle material that fractures easily during the necessary polishing and grinding steps for sample analysis. Eutectic composite materials often have improved strength through the inhibition of crack propagation.[13] In the PbTe-Ge materials reported previously and the PbTe-Si eutectic materials presented here the qualitative improvement in mechanical strength is apparent.[23] The eutectic samples show much improved machinability and crack resistance during cutting and polishing during sample preparation for transport measurements, SEM, and TEM analysis. Initial Vickers hardness measurements performed on several eutectic samples indicate the hardness (0.6−0.8 GPa) is significantly increased compared to PbI_2 doped PbTe itself (~0.3 GPa). Additional measurements to determine fracture toughness and other mechanical properties are underway and will be reported elsewhere.

Powder X-ray diffraction (PXRD) results indicate the presence of PbTe and Si phases in the samples. In addition, peaks corresponding to metallic Pb were observed, see Figure 1a. In several samples a broad amorphous reflection was also observed via powder X-ray diffraction. These broad reflections originate from the amorphous regions at the interface of the PbTe and Si precipitates as observed via transmission electron microscopy. Analysis of PbTe-Si(8%) by differential thermal analysis shows melting and crystallization transitions at 927 °C, a higher temperature than the published phase diagram indicates (900 °C),[25] Figure 1b,c. The band gap of the composite was measured to be 0.27 eV comparable to that of PbTe itself, Figure 1d.

Scanning electron microscopy was used to analyze the microstructure of the composite eutectic. Silicon precipitates were observed throughout regions of PbTe, Figure 2a,b. These rod-like precipitates, approximately 40−250 nm in diameter, appear to be several micrometers in length. The precipitates of Si are generally smaller than those observed in the PbTe-Ge system[23] (Ge precipitates tend to be several micrometers in diameter) and suggests that the crystallization of the PbTe-Si eutectic during quenching occurs faster and does not allow for the Si to migrate through the sample to form larger precipitates. Traces of Pb metal were observed via PXRD and in scanning electron microscopy as ~20 μm precipitates, although these precipitates were very few in number and separated from each other.

Investigations by transmission electron microscopy (TEM) identified additional Pb precipitates of 2−20 nm

(26) Ankudinov, A. L.; Ravel, B.; Rehr, J. J.; Conradson, S. D. *Phys. Rev. B* **1998**, *58*(12), 7565–7576.

(27) Ren, F.; Hall, B. D.; Ni, J. E.; Case, E. D.; Sootsman, J.; Kanatzidis, M. G.; Lara-Curzio, E.; Trejo, R. M.; Timm, E. J. *Mater. Res. Soc. Symp. Proc.* **2008**, *1044*, 121.

(28) Gelbstein, Y.; Gotesman, G.; Lishzinker, Y.; Dashevsky, Z.; Dariel, M. P. *Scr. Mater.* **2007**, *58*(4), 251–254.

(29) Gelbstein, Y.; Dashevsky, Z.; Dariel, M. P. *J. Appl. Phys.* **2008**, *104*(3), 033702/1–033702/4.

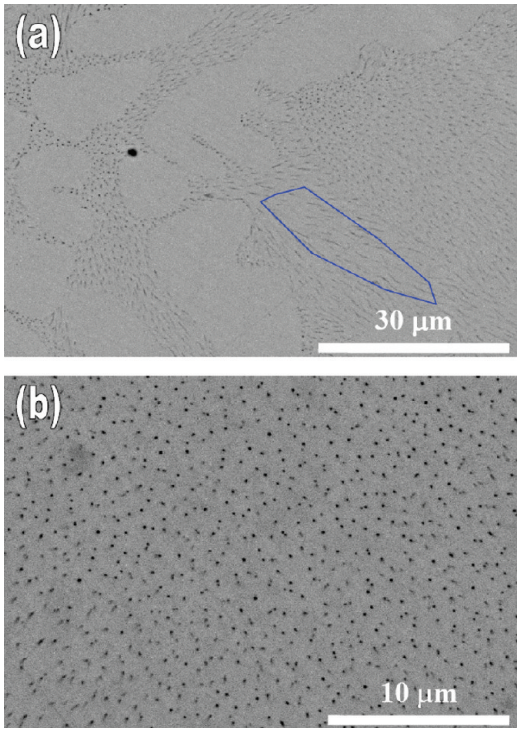

Figure 2. Scanning electron micrographs of PbTe-Si(8%) indicating (a) the rodlike morphology of the Si precipitates ~40−200 nm in diameter. (b) Indicates the relatively narrow size distribution of the diameter of the Si precipitates. Blue outlined region distinguishes precipitates observed perpendicular to the smaller diameter.

in diameter located in the PbTe domains of the samples. TEM revealed that, within the material, several regions exist including the PbTe matrix with Si precipitates (Figure 3a), PbTe with Pb nanoprecipitates (Figure 3b, c), and a boundary layer between the matrix and Si. The Si precipitates are observed as light colored regions (~80−150 nm) in the bright field image due to their significantly lower atomic number compared to PbTe. The boundary layer between the Si precipitates and the PbTe matrix (~2−5 nm thickness) will be discussed in greater detail below. The Pb nanoprecipitates (~2−20 nm) have a darker contrast than the matrix PbTe; however, no additional reflections were observed via selected area electron diffraction, Figure 3d. Only the matrix reflections along the [001] axis were observed reflections from precipitates could not be detected because of the very small volume fraction in the selected area. Similar observations were made in the PbTe-Ge-(20%) eutectic system where Ge displaced Pb in the PbTe matrix giving rise to a small percentage of $Pb_{1-x}Ge_xTe$ solid solution and Pb precipitates. The Pb nanoprecipitates are the result of Si displacing Pb to form Si_2Te_3 at the interface between the PbTe and Si phases according to the redox reaction of eq 1.

$$0.92\mathrm{PbTe} + 0.08\mathrm{Si} \rightarrow (0.92 - x)\mathrm{PbTe} + \left(0.08 - \frac{2x}{3}\right)\mathrm{Si} + (x)\mathrm{Pb} + \left(\frac{x}{3}\right)\mathrm{Si_2Te_3} \quad (1)$$

In contrast to the Ge system, where a stable $Pb_{1-x}Ge_xTe$ solid solution is formed, there is little solubility of

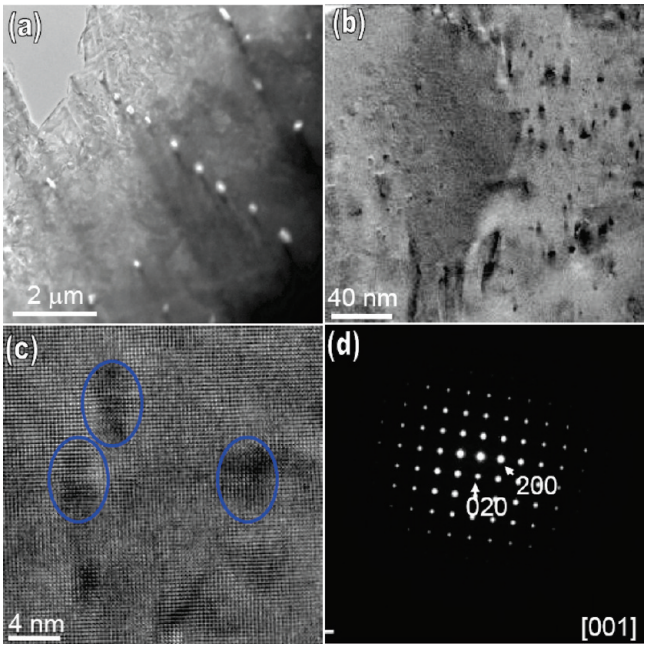

Figure 3. (a) Low magnification TEM image showing Si precipitates (white spots) embedded in the PbTe matrix. (b) TEM image showing the matrix PbTe material containing Pb nanoprecipitates. (c) High resolution TEM micrograph of several Pb precipitates with a size of 2−5 nm in dark contrast and (d) electron diffraction pattern with an aperture only including the Pb precipitates and PbTe matrix showing the [001] axis of the PbTe matrix.

Si in PbTe and the resulting Si−Te phase is trapped at interparticle boundaries. The only known Si−Te compound is Si_2Te_3 and is likely present at the boundaries between Si and PbTe as Si_2Te_3 has limited solubility in both PbTe and Si.[25] This boundary phase may decompose upon exposure to water during sample preparation and appear as a glassy interfacial film at the surface of Si precipitates embedded in the PbTe matrix. One representative precipitate is shown in Figure 4a along with a high resolution image of the boundary, Figure 4b. At the surface of the silicon precipitates the crystalline Si_2Te_3 was readily hydrolyzed upon exposure to water during sample preparation forming glassy SiO_x and H_2Te. The presence of oxygen at this amorphous boundary was confirmed using EELS measurements, Figure 4c. The results of our EELS calculations, curve 4 in Figure 4c, confirm the two oxygen peaks both come from SiO_x. It is likely that this Si_2Te_3, when embedded in the bulk material, is stable and may act as an interface to allow charge transport between the PbTe and Si.

Electrical and Thermal Transport Characterization. Room temperature electrical conductivity and Seebeck coefficient measurement results are summarized for a series of PbTe-Si(8%) doped with PbI_2 in Figure 5. The electrical conductivity increased monotonically with PbI_2 concentration as expected for a rising carrier concentration. At room temperature the electrical conductivity was 390 S/cm for the sample without PbI_2, and it increased linearly to 2750 S/cm for the sample doped with 0.08 mol % PbI_2. The corresponding Seebeck coefficient is negative (n-type) and decreased from −200 μV/K to −80 μV/K for the same PbI_2 concentrations. A large power factor at room temperature

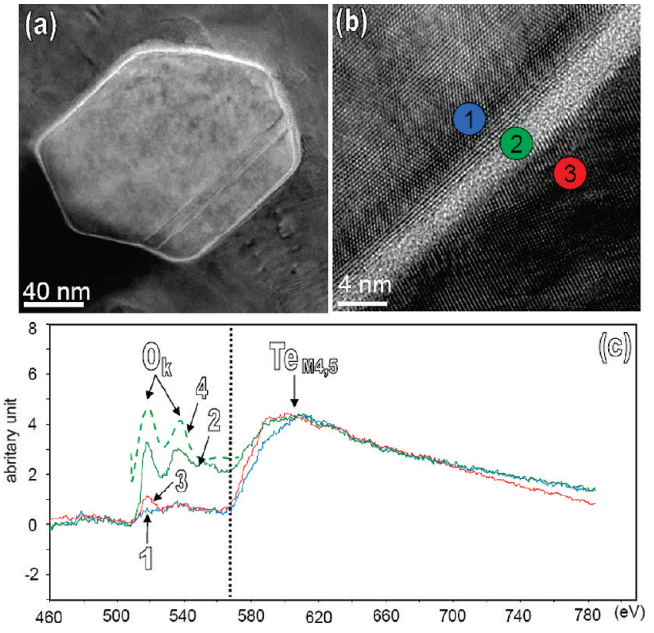

Figure 4. (a) Medium magnification TEM image containing one Si precipitate; (b) high resolution TEM micrograph of the amorphous glassy SiO_x interface phase between the PbTe and Si precipitate (region 1 is the Si, region 2 the boundary, and region 3 the PbTe). (c) EELS spectrum showing the presence of oxygen in the glassy SiO_x interface. The number labels in the spectrum correlate to those shown in (b). EELS spectrum (line 4) is from multiple-scattering calculation of oxygen K edge in SiO_2.

(~36 μW/(cm K^2)) was obtained for the optimized carrier concentration of 7.71 × 10^{18} cm^{-3} in the 0.025% PbI_2 doped sample.

Temperature dependent electrical conductivity, Seebeck coefficient, power factor, and lattice thermal conductivity for a series of PbI_2 doped PbTe-Si(8%) materials are shown in Figure 6. All samples show a decreasing electrical conductivity with increasing temperature consistent with common scattering mechanisms in PbTe based materials.[30] The Seebeck coefficient increases in magnitude with rising temperature, and for certain doping concentrations reaches ~−300 μV/K at temperatures >650 K. This behavior is comparable to pure n-type PbTe.[31] The power factor remains high (>15 μW/(cm K^2)) at these temperatures and contributes to the moderate ZT observed.

Generally, the thermal conductivity is comprised of two components: the lattice and electronic thermal conductivity ($\kappa_{tot} = \kappa_{lat} + \kappa_{elec}$). According to the Wiedemann−Franz law the electronic component is calculated to be $\kappa_{elec} = L\sigma T$ where L is the Lorenz number, σ the electrical conductivity, and T the temperature.[32] Initially, the electronic thermal conductivity was calculated using the Lorenz number for metals and heavily degenerate semiconductors ($L_0 = 2.45 \times 10^{-8}$ (W Ω)/K^2). When this method was used, a wide range of the lattice thermal conductivity values from 0.7 W/mK to 1.2 W/mK at high temperatures were calculated, Figure 6d. This result was unexpected as there were only small differences in the

(30) Yu, I.; Ravich, B. A. E.; Smirnov, I. A. *Semiconducting Lead Chalcogenides*; Plenum Press: New York, 1970; Vol. 5.
(31) Dughaish, Z. H. *Physica B* **2002**, *322*(1−2), 205–223.
(32) Kittel, C. *Introduction to Solid State Physics*, 8th ed.; John Wiley & Sons: New York, 2005.

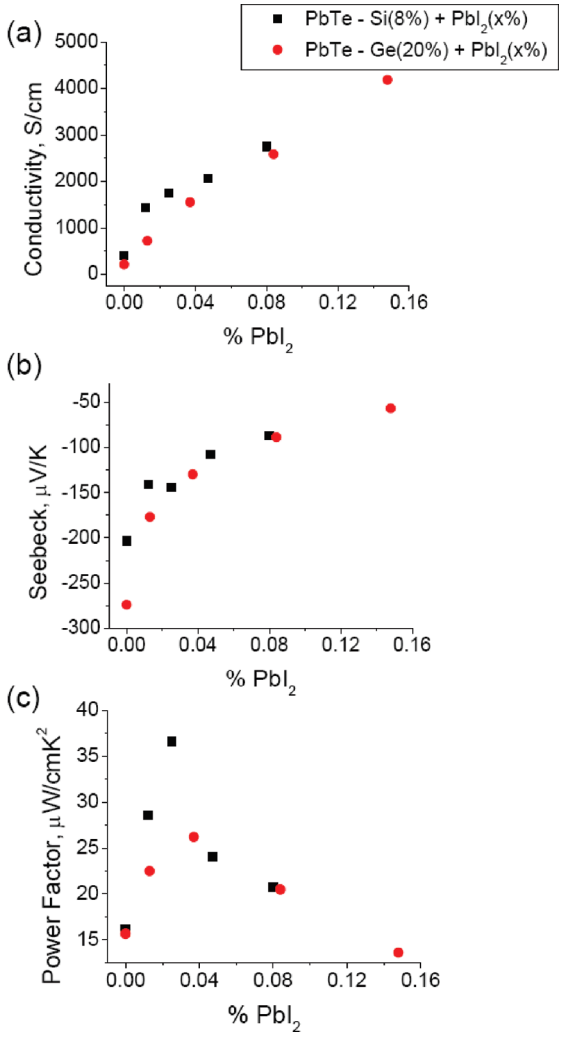

Figure 5. Comparison of the room temperature (a) electrical conductivity, (b) Seebeck coefficient, (c) and power factor for PbI_2 doped eutectic materials of PbTe-Ge(20%) and PbTe-Si(8%). Generally, the uncertainly in the electrical conductivity data is ~±2−3% whereas in the Seebeck coefficient data were within ±5%.

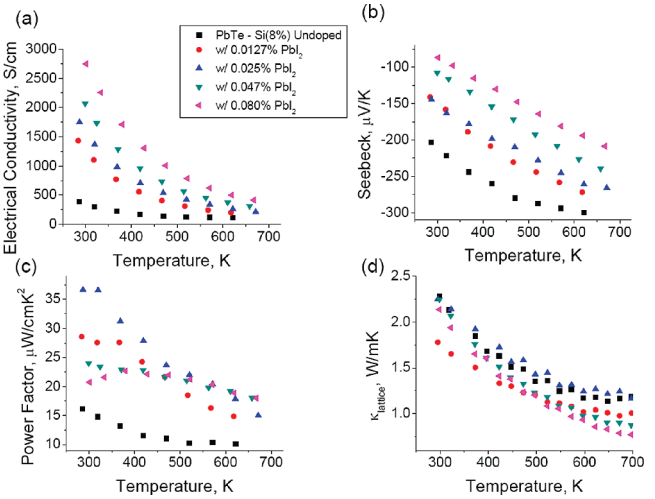

Figure 6. Temperature dependent (a) electrical conductivity, (b) Seebeck coefficient, (c) power factor, and (d) lattice thermal conductivity for a series of PbTe-Si(8%) doped with PbI_2.

PbI_2 dopant concentration between the samples that would not account for the large change in lattice thermal

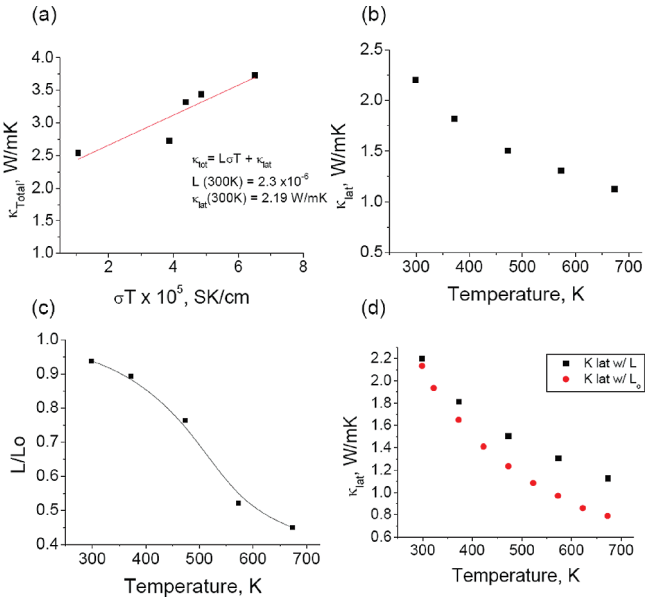

Figure 7. (a) Room temperature total thermal conductivity fit as a function of σT, (b) calculated lattice thermal conductivity, (c) ratio of calculated L/L_0 as a function of temperature, and (d) a comparison of the lattice thermal conductivity using L and L_0 showing the significant underestimate when L_0 was used.

conductivity observed. This suggested that the assumption that L is constant with temperature is incorrect. In fact, theoretical estimates of the Lorenz number in n-type PbTe show that in the range of interest (300−700 K and 10^{18}−10^{19} cm^{-3} carriers) the Lorenz number is lower than L_0 because of nonelastic scattering as well as band nonparabolicity resulting in a Lorenz number of only 55% of L_0 at 700 K.[33]

To estimate a more correct Lorenz number and better determine the lattice thermal conductivity in these materials, the total thermal conductivity was plotted as a function of σT. From this, the equation $\kappa_{tot} = \kappa_{lat} + L\sigma T$ was fit, and the lattice thermal conductivity and L were extracted from the intercept and the slope of the linear fit. A representative example is shown in Figure 7a for the data at 300 K. This procedure was repeated for several temperatures between 300 and 700 K using the same linear fit to approximate the Lorenz number and lattice thermal conductivity at each temperature. The Lorenz number determined in this manner is shown as a ratio with L_0 in Figure 7c. At 300 K the ratio is close to 1 indicating that the material can be described by the Wiedemann−Franz law using the Lorenz number for metals. At high temperatures a significant deviation from L_0 is observed which shows that the lattice thermal conductivity is greatly underestimated when a Lorenz number of 2.45×10^{-8} (W Ω)/K^2 is used, Figure 7d. In this crude approximation several effects including electron phonon interactions are neglected; however, it is apparent that in many PbTe-based materials using L_0 in calculations can lead to greatly underestimated lattice thermal conductivity values. In addition, the Lorenz number also depends on the carrier concentration, and so the

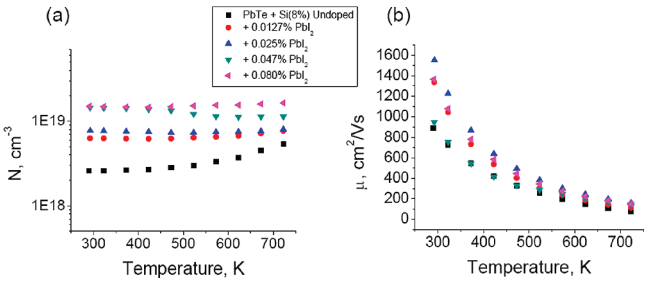

Figure 8. (a) Hall effect derived carrier concentrations as a function of temperature and (b) the temperature dependent mobility for a series of PbTe-Si(8%) samples doped with PbI_2.

estimates of the lattice thermal conductivity determined in this manner are approximate. Regardless of the lattice thermal conductivity calculated, the value of the total thermal conductivity is a measured quantity and is used in the calculation of ZT.

The lattice thermal conductivity obtained from these fits is shown in Figure 7b indicating that the lattice thermal conductivity follows closely the expected values for PbTe itself[31] and follows the $1/T$ dependence predicted from theory.[34] In the PbTe-Si(8%) samples the expected lattice thermal conductivity of the composite is 2.36 W/mK at room temperature as calculated by effective medium theory.[35] Although the thermal conductivity of Si is much higher (∼130 W/mK) than that of PbTe (∼2.2 W/mK) the volume fraction of Si is low, and the increase in lattice thermal conductivity only amounts to a 7% increase from that of PbTe.

High temperature Hall effect measurements were used to calculate the carrier concentration as a function of temperature. The obtained values are shown in Figure 8a for the PbTe-Si(8%) samples doped with PbI_2. The carrier concentration is stable as a function of temperature with the exception of the undoped sample. In this sample the carrier concentration increased as the temperature increased, likely due to carrier excitation. At very high temperatures (>800 K) the samples showed some increase in carrier concentration that in certain cases persisted upon cooling perhaps as a result of Pb precipitates dissolving or changes in Si doping in the PbTe matrix. However, in all measurements of electrical conductivity, Seebeck coefficient, and thermal conductivity up to ∼700 K, the sample remained stable for several heating and cooling cycles.

The temperature dependent electron mobility was determined from the Hall and electrical conductivity measurements. At room temperature the mobility in these materials remains high (∼900−1500 $cm^2/(V\ s)$) and decreases according to the power law $\mu \sim aT^{\alpha}$ where α = 1.8−2.3, Figure 8b. The mobility and its temperature dependence are typical of pure PbTe despite the precipitates of Pb and Si throughout the sample.[30,31,36] It is

(33) Vineis, C. J.; Harman, T. C.; Calawa, S. D.; Walsh, M. P.; Reeder, R. E.; Singh, R.; Shakouri, A. *Phys. Rev. B* **2008**, *77*(23), 235202/1–235202/14.
(34) Keyes, R. W. *Phys. Rev.* **1959**, *115*, 564–567.
(35) Wang, J.; Carson, J. K.; North, M. F.; Cleland, D. J. *Int. J. Heat Mass Transfer* **2008**, *51*(9−10), 2389–2397.
(36) Efimova, B. A.; Kolomoets, L. A.; Ravich, Y. I.; Stavitskaya, T. S. *Fizika i Tekhnika Poluprovodnikov* **1970**, *4*(10), 1929–1935.

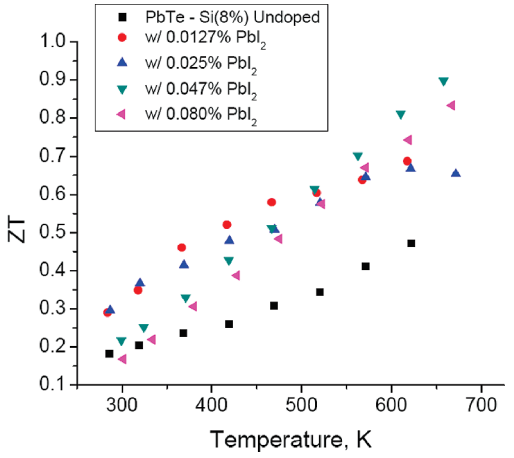

Figure 9. ZT as a function of temperature for a series of PbTe-Si(8%) doped with PbI_2.

possible that the boundary phase between the PbTe and Si is responsible for allowing charge transport through the composite. It is also possible that there is an additive effect where the transport through the Si microprecipitates is facile and improves the overall composite mobility. In the previously reported PbTe with Pb precipitates the mobility was significantly degraded;[37] however, such a scattering process does not appear to occur in our samples or is masked by the high mobility through the Si rods. Additionally, in the PbTe-Pb system the Seebeck coefficient increased with respect to PbTe itself, although with an overall decrease in power factor.[37] The PbTe-Si eutectic composites show very similar Seebeck coefficients as PbI_2 doped PbTe[36] without any increase in the Seebeck coefficient regardless of the Pb nanoprecipitates within the PbTe-Si composite.

The resulting ZT as a function of temperature is shown in Figure 9. A maximum ZT of 0.9 at 660 K was obtained for the sample doped with 0.047% PbI_2 ($N = 1.13 \times 10^{19}$ cm^{-3}). The trends in ZT shown in Figure 9 suggest the figure of merit could exceed 1 at ~800 K. This value is similar to PbTe itself; however, as we reported previously further increases were attained when Si was alloyed with Ge to reduce the thermal conductivity.[38] For the PbTe-$Si_{0.8}Ge_{0.2}$(8%) doped with PbI_2 the ZT was increased to 1.2 at 700 K because of a reduction of thermal conductivity, similar to the previously reported PbTe-$Ge_{0.8}Si_{0.2}$-(5%) composite.[23]

Concluding Remarks

The micro- and nanostructure in the eutectic composition PbTe-Si(8%) influences the electrical and thermal transport so that the ZT remains high in these materials. The electrical transport properties are tuned by n-type doping with PbI_2, and the resulting thermoelectric properties are comparable to PbTe itself, but with considerably reduced brittleness. The lattice thermal conductivity was not significantly influenced by the presence of Si or Pb precipitates. This indicates it may be possible to use secondary phases embedded in thermoelectric materials to significantly increase their mechanical strength without influencing the thermoelectric performance if selected judiciously. The Lorenz number in these materials is not constant over the temperatures measured and can greatly influence the calculation of the electronic contribution to the thermal conductivity. Attempts to dope this system p-type are underway and will be reported elsewhere. If suitable eutectic materials can be prepared using both p- and n-type dopants, their improved mechanical properties compared to PbTe and ease of synthesis make them attractive for large scale device fabrication.

Acknowledgment. Financial support from the Office of Naval Research is gratefully acknowledged. Portions of the scanning electron microscopy work was performed in the (EPIC) (NIFTI) (Keck-II) facility of NUANCE Center at Northwestern University. NUANCE Center is supported by NSF-NSEC, NSF-MRSEC, Keck Foundation, the State of Illinois, and Northwestern University.

(37) Heremans, J. P.; Thrush, C. M.; Morelli, D. T. J. Appl. Phys. **2005**, *98* (6).

(38) Dismukes, J. P.; Ekstrom, L.; Steigmeier, E. F.; Kudman, I.; Beers, D. S. *J. Appl. Phys.* **1964**, *35*(10), 2899–2907.